Non-invasive characterization of normal and pathological tissues through dynamic infrared imaging in the hamster cheek pouch oral cancer model

María S. Herrera[a], Andrea Monti Hughes[c], Natalia Salva[b,d], Claudio Padra[b,d], Amanda Schwint[b,c], and Gustavo A. Santa Cruz[c]

[a]CETMIC, CIC-CONICET-CCT La Plata, Camino Centenario y 506, M. B. Gonnet, B1897ZCA, Argentina
[b]CONICET, Godoy Cruz 2290, Buenos Aires, C1425FQB, Argentina
[c]Comisión Nacional de Energía Atómica, Av. Gral. Paz 1499, Buenos Aires, B1650KNA, Argentina
[d]Comisión Nacional de Energía Atómica, Av. Bustillo 9500, Bariloche, 8400, Argentina

ABSTRACT

Biomedical infrared thermography, a non-invasive and functional imaging method, provides information on the normal and abnormal status and response of tissues in terms of spatial and temporal variations in body infrared radiance. It is especially attractive in cancer research due to the hypervascular and hypermetabolic activity of solid tumors. Moreover, healthy tissues like skin or mucosa exposed to radiation can be examined since inflammation, changes in water content, exudation, desquamation, erosion and necrosis, between others, are factors that modify their thermal properties.

In this work we performed Dynamic Infrared Imaging (DIRI) to contribute to the understanding and evaluation of normal tissue, tumor and precancerous tissue response and radiotoxicity in an *in vivo* model, the hamster cheek pouch, exposed to Boron Neutron Capture Therapy. In this study, we particularly focused on the observation of temperature changes under forced transient conditions associated with mass moisture transfer in the tissue-air interface, in each tissue with or without treatment. We proposed a simple mathematical procedure that considerers the heat transfer from tissue to ambient through convection and evaporation to model the transient (exponential decay o recover) thermal study. The data was fitted to determined the characteristic decay and recovery time constants of the temperature as a function of time. Also this model allowed to explore the mass flux of moisture, as a degree of evaporation occurring on the tissue surface. Tissue thermal responses under provocation tests could be used as a non-invasive method to characterize tissue physiology.

Keywords: Dynamic infrared imaging, Boron Neutron Capture Therapy, Hamster cheek pouch, Oral cancer, Oral precancer, Mucositis, Diffusion model, Heat equation

Corresponding author E-mail: mherrera@cetmic.unlp.edu.ar

Thermosense: Thermal Infrared Applications XXXIX, edited by Paolo Bison, Douglas Burleigh, Proc. of SPIE
Vol. 10214, 102140D · © 2017 SPIE · CCC code: 0277-786X/17/$18 · doi: 10.1117/12.2264426

NOMENCLATURE

$\alpha = k/\rho C_p$	Thermal diffusivity
Δr_s	Thickness of the cheek pouch
δ	Fixed positive temperature difference
κ	Constant given by Eq. (9)
$\lambda = \lambda_W + \lambda_s$	Latent heat of vaporization plus heat of sorption
μ	Constant given by Eq. (10)
ρ	Tissue density
τ	Characteristic time constant
C_p	Specific heat capacity
D	Diffusion coefficient
h	Heat transfer coefficient between superficial tissue and air
J	Mass flux of moisture
k	Thermal conductivity of the tissue
Nu	Nusselt number
P	Probability
Q	Total heat transfer
r	Distance from the center of a symmetrical cylindrical region
t	Time
$T = T(r,t)$	Temperature distribution in the tissue
T^*	Dimensionless temperature of the tissue
T_∞	Final (asymptotic) temperature of the tissue
T_i	Initial temperature of the tissue
T_{amb}	Ambient temperature
$X = X(r,t)$	Moisture content in tissue
Subscripts	
int	Inner surface of the layer
s	Outer surface of the layer
Abbreviations	
BNCT	Boron Neutron Capture Therapy
BO	Beam Only
BPA	Boronophenylalanine
CICUAL-CNEA	National Atomic Energy Commission Animal Care and Use Committee
CNEA	Argentine National Atomic Energy Commission
DIRI	Dynamic Infrared Imaging
DMBA	Dimethylbenzanthracene
IR	Infrared
IRT	Infrared Thermography
LET	Linear Energy Transfer
PT	Provocation Test
ROI	Regions Of Interest
RP	Recovery Phase
TEP	Transient Equilibrium Phase

1. INTRODUCTION

Over the past ten years, technological advances in infrared cameras in resolution, thermal sensitivity, signal-to-noise and image acquisition speed has allowed to quantitatively assess thermal patterns. Employing radiometric measurements and algorithms that convert infrared radiance to temperature, the thermography technique can be used to quantify temperature distribution on body surfaces and to correlate thermal physiology with skin temperature.[1–3] The spatial and temporal pattern of temperature generated, depending on physical parameters such as emissivity coefficient or thermal conductivity, is determined by internal factors such as metabolic, inflammatory and homeostatic processes and also external factors.[4] In particular, thermography it is especially attractive in cancer research due to the hypervascular and hypermetabolic activity of solid tumors[5] . Moreover, healthy tissues like skin or mucosa exposed to radiation can be examined since inflammation, changes in water content, exudation, desquamation, erosion and necrosis, between others, are factors that modify their thermal properties.[4] In medicine, thermal imaging has been used for more than 50 years in various clinical settings.[6]

Boron Neutron Capture Therapy (BNCT) is a binary treatment that combines the administration of boron carriers that are taken up preferentially by neoplastic tissue and irradiation with a thermal or epithermal neutron beam (with energies of the order of eV and keV, respectively). The high Linear Energy Transfer (LET) alpha particles (^{4}He) and recoiling lithium-7 (^{7}Li) nuclei emitted during the capture of a thermal neutron by a boron-10 (^{10}B) nucleus have a higher killing efficiency compared to X-rays or gamma photons. Their short range in tissue (6-10 μm) would limit the damage largely to cells containing ^{10}B. In this way, BNCT would target neoplastic tissue selectively, sparing normal tissue.[7]

As part of the BNCT project conducted by the Argentine National Atomic Energy Commission (CNEA), Dynamic Infrared imaging (DIRI) has been included in different research protocols involving small animals, for the purpose of providing non-invasively supplementary *in vivo* information potentially useful to characterize of normal and pathological tissues and their response to the therapy.[3] DIRI was previously proposed[1] as a method to maximize the thermography information. The technique is based on the acquisition of thermal images during transient processes, caused by sudden and sustained changes in surface temperature due to the application of a thermal stimulus (provocation test) that forces the neurovascular system to respond in order to maintain local and body temperature within normal parameters.[8] Other authors followed this concept, including our group,[2,3] in different clinical research studies using thermography.[9–12]

Squamous Cell Carcinoma of the Head and Neck (SCCHN) is the sixth most common cancer worldwide; approximately 600,000 new cases are diagnosed per year worldwide.[13] The most frequent tumor sites are the larynx, pharynx and the oral cavity.[14] It is often radio-/chemo-resistant and show extensive growth.[15] BNCT was previously proposed as a head and neck cancer therapy to avoid severe impairment of oro-facial structures and functions, showing promising results.[15]

Crandell and Hill were the first researchers to publish data on the use of infrared thermography (IRT) in dental research.[4] In 1971, Irwin et al. applied IRT to the intra-oral environment.[16] They found that useful images can be produced by real-time thermographic systems and that these in turn should be useful in screening for cancer, management of burn/wound healing, surgery and prosthodontics. White et al. also examined a small number of individuals thermographically and suggested that IRT may provide a means to assess the degree of oral mucosal inflammation.[17]

The hamster cheek pouch model of oral cancer was previously proposed by our group for experimental BNCT studies,[18,19] and preceded the first clinical trial of BNCT for head and neck malignancies.[15] In 2012, we studied DIRI in this hamster cheek pouch model, and observed that the temperature of the hamster cheek pouch, in certain cases, is below ambient temperature and always lower than body core temperature.[3] The former case could be explained by superficial water evaporation, producing this cooling effect.

In the present work we combined DIRI with theoretical and experimental studies to thermally characterize tumor, precancerous and normal tissue in the hamster cheek pouch oral cancer model, with or without BNCT. We focused on the observation on temperature changes under transient conditions associated with mass moisture transfer in the tissue-air interface. Thermal responses in the tissues were assessed before, during and after the application of a thermal stimulus (provocation test) that forces temperature changes at the interface.

2. EXPERIMENTAL PROCEDURE

2.1 Biological model

The golden Syrian hamster, *Mesocricetus auratus*, has an anatomic feature that can be use to our advantage, i.e. a pocket within the thickness of the cheek on each side, which only communicates with the oral cavity at the corners of the mouth and is lined with stratified squamous epithelium which resembles that of the oral cavity.[20] The hamster cheek pouch is easily accessible *in situ* and can be easily everted and extended for irradiation and follow up.[20] It is a widely accepted model of oral cancer.[18,21] Carcinogenesis protocols induce premalignant and malignant changes that closely resemble spontaneous human oral mucosa lesions.[18,20–22] The mode of tumor induction provides a model of tumor surrounded by a field-cancerized tissue. Field cancerization refers to the existence of transformed cells in areas adjacent to the primary tumor.[23] Different terms have been used to refer to oral mucosa that can give rise to the development of multiple oral tumours, e.g. precancerous tissue, premalignant tissue.[24] The relevance of field cancerization in head and neck cancer lies in the frequent occurrence of second primary tumors after treatment.[20,25] In addition, the dose-limiting nature of field-cancerized tissue must be considered. The hamster cheek pouch is also a widely accepted model of oral mucositis.[26] In a clinical scenario, confluent oral mucositis is a frequent, dose-limiting side effect during conventional radiotherapy[27] and is a consideration in BNCT for advanced head and neck cancers.[28,29] Oral mucositis is the painful inflammation and ulceration of the mucous membranes lining the oral cavity, usually as an adverse effect of cancer treatment,[30] that causes significant pain. The lesion can also be detrimental to diet, nutrition, oral hygiene, and quality of life. In certain cases, the significant morbidity associated with oral mucositis may cause dose reductions, delays, and/or treatment interruptions in cancer therapy which in turn can jeopardize therapeutic efficacy.[27] Also, oral mucositis could enhance tumorigenesis.[24,31] Nowadays, oral mucositis continues to represent an important unmet medical need.[32]
We previously demonstrated in the oral cancer model, the BNCT therapeutic efficacy on tumors[7,19] and its inhibitory effect on tumor development in precancerous tissue.[33] We employed boron compounds approved for their use in humans such as boronophenylalanine (BPA)[7] and novel boron compounds.[34] However, BNCT induced mucositis in precancerous tissue.[24] Based on clinical and animal research observations, it becomes necessary to have a complementary and non invasively method to perform a macroscopic inspection that could describe in more detailed tumor, precancerous and normal tissue response to BNCT, in terms of tumor development and mucositis.

2.2 Tumor induction and radiobiological studies

The right cheek pouches of non-inbred hamsters were treated with a topical application of 0.5 % carcinogen Dimethylbenzanthracene (DMBA; Sigma Chemical Co., San Luis, MO, USA) in mineral oil. They were exposed to two cancerization protocols: -Protocol 1- DMBA application for 6 weeks, to study precancerous tissue[22] and -Protocol 2- DMBA application for 12 weeks, to study tumor and precancerous tissue.[35] Protocol 2 induces a very aggressive and hypersensitive precancerous tissue that gives rise in turn to multiple tumors, allowing short-term follow up (1 month). Instead, Protocol 1, induces a less aggressive precancerous tissue, mimicking human oral carcinogenesis more closely. It allows for the study of the BNCT inhibitory effect on the development of new tumors at longer-term studies (8 months).[24] The cancerized pouches were exposed to BNCT mediated by BPA (BPA-BNCT) and BO, i.e., neutron irradiation without BPA administration to study the effect of background dose. We also treated non cancerized (normal) animals with BPA-BNCT to assess the effect of BNCT on normal tissue.[36] The animals were irradiated at the RA-6 nuclear reactor located at Bariloche, Argentina. BPA-Fructose (0.14 M) was administered intravenously [iv., 15.5mg ^{10}B/kg body weight (b.w.)]. The animals were irradiated 3 hours post BPA injection. Boron concentration values and irradiations conditions can be found in detail in.[36]

Finally, a group of cancerized animals with no treatment was also included as a control group.

Animal experiments were carried out in accordance with the Guidelines laid down by the National Institute of Health in the USA regarding the care and use of animals for experimental procedures and in accordance with protocols approved by the National Atomic Energy Commission Animal Care and Use Committee (CICUAL-CNEA).

2.3 DIRI experiments

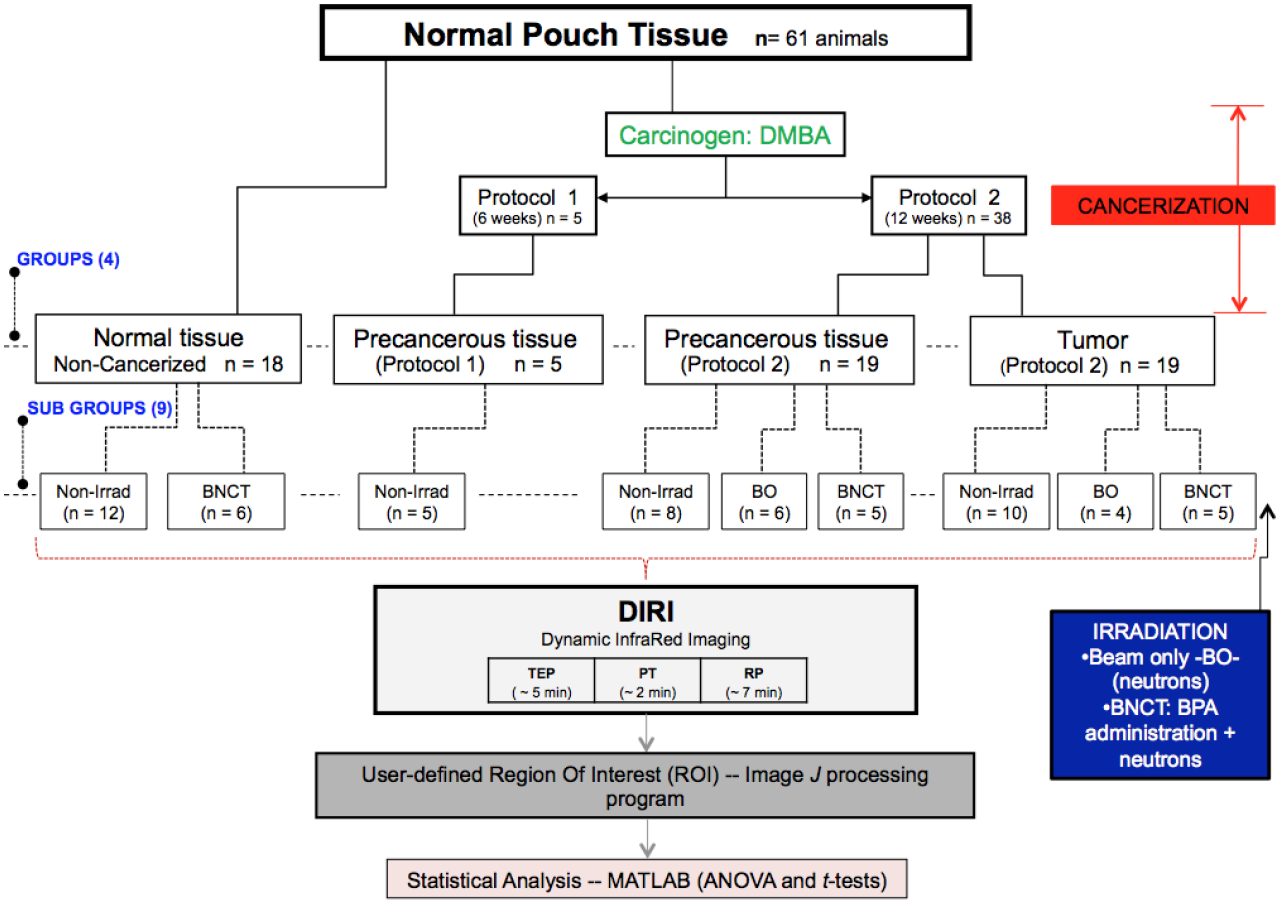

Figure 1: 61 animals were used to study the thermal responses of normal (non-cancerized) tissue, precancerous tissue cancerized with protocol 1, precancerous tissue and tumors induced by protocol 2 (4 groups). Also if they were treated with BNCT, Beam Only (BO), or Non-irradiated (Non-irrad) (9 sub-groups). All groups were examined under DIRI protocol. Regions of interest were defined in each image using the Image J software. Data was processed and analyzed with MATLAB®. According to the case, a statistical analysis was performed (t-test or ANOVA).

A total of 61 hamsters were examined under DIRI protocol, divided into 9 groups as is shown in Figure 1. Following an acclimatization period of 10 minutes in the room, the animals were anesthetized (iv., ketamine 140 mg/kg b.w. and xilazine 21 mg/kg b.w.) and the pouch was everted using a plastic pipette held by hand (Figure 2). Since the pipette is void inside, a thermocouple was positioned inside the pipette and used to measure the temperature as an inner boundary condition. For each group, thermal responses were measured before, during and after the provocation test, namely, Transient Equilibrium Phase (TEP), Provocation Test (PT) and Recovery

Phase (RP), respectively. The PT consisted of a mild air current applied at ambient temperature for about 120 seconds. The purpose of an air stimulus is to eliminate the initial moisture condition of the tissue so that, in the RP, we can focuse on its thermal behaviour and evaporation process that occur in response of the PT. In TEP and RP no air was applied, leaving the pouch exposed to ambient conditions without perturbations during approximately 280 and 400 seconds, respectively. The irradiated groups were evaluated with DIRI at 1 week post irradiation.

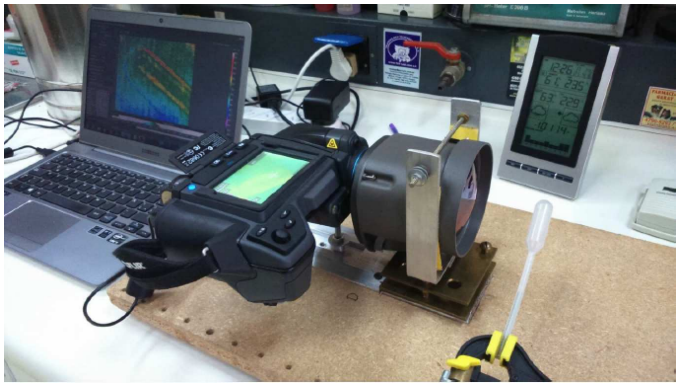

Figure 2: Imaging system showing the infrared camera, instruments and the pipette used to evert the hamster cheek pouch. An optic zoom can be coupled to the camera to improve the spatial resolution (spacial scale: 1 pixel = 49 micrometers).

An air-conditioning device controlled the laboratory temperature (26 ± 2 °C). Temperature and relative humidity of the room were monitored during the experiments by a digital thermohygrometer. No incandescent lights were employed in the room. The IR camera was properly positioned to allow for a continuous observation of the evolution of tissue temperature during the whole procedure (Figure 2). The distance between the camera and the pouch was set up at 30 cm.

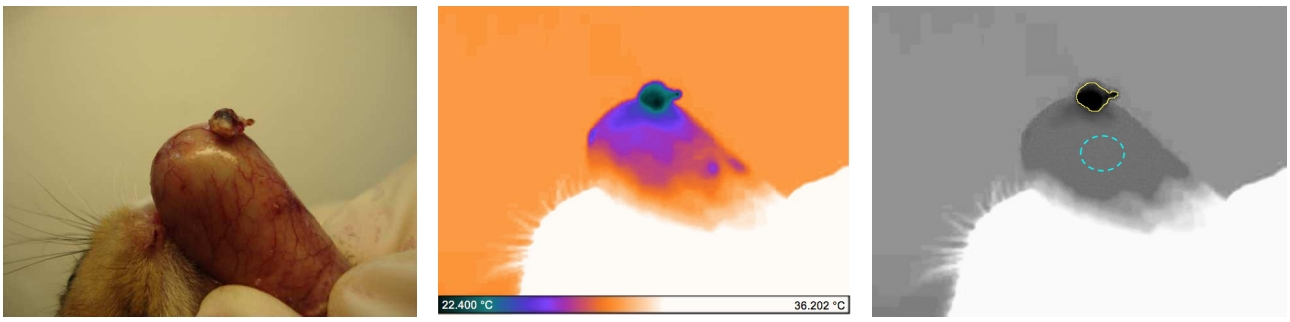

(a) Visible image. (b) IR image. (c) Digitized 8-bit image.

Figure 3: Example of a cancerized hamster cheek pouch bearing a tumor, surrounded by precancerous tissue. The Regions Of Interest (ROIs) are marked in the digitized image: solid yellow line for the tumor and cyan dashed line for a precancerous tissue region. Images were obtained during the provocation test (PT).

The thermography data were recorded using a FLIR T420 infrared (320×240 uncooled microbolometers) camera with a thermal sensitivity < 0.04 °C. The camera works in the spectral range of 7.5 to 13 μm. In the wavelength region above 3 micrometers, the tissue emissivity coefficient is almost constant, with values between

0.95 and 0.98.[16,37,38] Emissivity is also nearly unity for mucosa in this range.[16] In this work we set the emissivity value at 0.95 in all cases. Infrared images were captured every 14 seconds throughout the experiment. These sets of images were digitized to 8-bit and converted to indexed tiff stacks for direct temperature reading. As an example, Figure 3 shows a visible image of a cancerized cheek pouch bearing a tumor, surrounded by precancerous tissue and the corresponding IR and 8-bit images (during the PT). The measured temperature values during time were extracted from the thermal image in a user-defined region of interest (ROI) used to delineate the tumor or regions of precancerous or normal tissue. This procedure needs several manual adjustments, until a stable image and ROI are obtained. ROIs were marked using the Image J processing program (See Figure 3.c).

3. MATHEMATICAL MODEL

In this section we derived the methodology used for obtaining some specific parameters that characterized the transient (exponential decay o recover) thermal study. This parameters are the characteristic time constant, τ [s], and the mass flux of moisture, J [Kg m^{-2}s^{-1}], i.e., a degree of evaporation occurring on the tissue surface. A simple mathematical model that considers the heat transfer from tissue to ambient through convection and evaporation will be used to model the transient process described in Section 4.

3.1 Methodology for the determination of τ and J

The unsteady-state diffusion equation has been frequently adopted in describing processes in food technology that involve water migration, such as drying of bananas,[39] cereal grain[40] and potatoes,[41] among others. According to Fick's second law of diffusion, the moisture concentration X [kg m^{-3}] as a function of time t and distance r, measured from the center of a symmetrical cylindrical region and perpendicular to the air stream from the core, can be described in cylindrical coordinates by,

$$\frac{\partial X}{\partial t} = \frac{D}{r}\frac{\partial}{\partial r}\left(\frac{r\partial X}{\partial r}\right), \tag{1}$$

with D, the diffusion coefficient.
We assume that the temperature distribution T in the tissue can be described by the heat conduction equation in cylindrical coordinates without heat sources,

$$\frac{\partial T}{\partial t} = \frac{k}{\rho C_p}\frac{1}{r}\frac{\partial}{\partial r}\left(\frac{r\partial T}{\partial r}\right), \tag{2}$$

where k is the thermal conductivity, ρ is the tissue density and C_p the specific heat capacity. These constants determine the thermal diffusivity $\alpha = k/\rho C_p$, a specific quantity depending on the tissue properties.
The total heat transfer, Q, given by Eq. (3) gives a boundary condition for Eq. (2),

$$Q = h\,(T_{amb} - T_s) - \lambda J\,, \tag{3}$$

where h is the heat transfer coefficient between the outer surface layer and the ambient, and T_{amb} is the ambient temperature related with the air stream. $\lambda = \lambda_W + \lambda_s$, is the latent heat of vaporization plus heat of sorption, respectively. In Eq. (3) the radiative heat loss was not included.

Following the procedure described in Refs.,[39,42] if the moisture and temperature gradients are approximated by finite differences, at the outer layer of the tissue we have,

$$\frac{dX_s}{dt} = \frac{1}{r}\frac{1}{\Delta r_s}\left(\frac{D\,r\,(X_{int} - X_s)}{\Delta r_s} - r\,J\right) \tag{4}$$

$$\frac{dT_s}{dt} = \frac{1}{r}\frac{1}{\Delta r_s \rho C_p}\left(\frac{k\,r\,(T_{amb} - T_s)}{\Delta r_s} + r\,Q\right), \tag{5}$$

where the subscripts s and int denote the outer and inner surfaces of the layer, respectively, and Δr_s is the thickness of the cheek pouch. The mass flux of moisture, J, is directly proportional to the difference between air humidity just above the most superficial layer of tissue and that in the bulk air stream.[39]

We considered that diffusion at the superficial layer is almost stationary. We assumed that the mild convective conditions (air current at ambient temperature) do not perturb the moisture profile within the tissue. Thus,

$$\frac{1}{r}\frac{1}{\Delta r_s}\left(\frac{D\,r\,(X_{int}-X_s)}{\Delta r_s}-r\,J\right)\simeq 0 \quad \Rightarrow \quad J\simeq\frac{D\,(X_{int}-X_s)}{\Delta r_s}\,. \tag{6}$$

Then, the temperature distribution given in Eq (5) can be expressed as,

$$\frac{dT_s}{dt}=\frac{1}{\rho C_p {\Delta r_s}^2}\left(k\,(T_{int}-T_s)+\Delta r_s\,(h\,(T_{amb}-T_s)-\lambda J)\right)\,. \tag{7}$$

Now we need to consider the internal boundary condition. We can assume either that it is a function of time, fixed or related with T_s. In this approach, no time dependence will be assumed. We will consider immediate thermal equilibrium through the tissue layer. This is, $T_{int}\simeq T_s+\delta$, where δ is a fixed positive temperature difference, this means that the internal temperature is higher than the external temperature and follows the average external temperature. This was experimentally observed with the internal thermocouple inside the pipette. Thus, Eq. (7) takes the simple form of,

$$\frac{dT_s}{dt}=\kappa T_s+\mu\,, \tag{8}$$

where

$$\kappa=\frac{h}{\rho C_p\Delta r_s} \tag{9}$$

$$\mu=\frac{k\,\delta+\Delta r_s h T_{amb}-\Delta r_s\lambda J}{\rho C_p {\Delta r_s}^2}\,. \tag{10}$$

The solution of the temperature as a function of time can be easily obtained integrating Eq. (8) and applying the initial condition $T_s(t=0)=T_i$. Then, the tissue temperature varied exponentially with time determined by the time constant τ according to,

$$T_s(t)=(T_i-T_\infty)\,e^{-\kappa t}+T_\infty\,. \tag{11}$$

with T_∞, the asymptotic temperature and,

$$\tau=\frac{1}{\kappa}\,. \tag{12}$$

Expression (11) will be used to fit the experimental data of temperature as a function of time measured in a given ROI with the method of least squares. The parameter τ will be determined in each phase of the study (TEP, PT and RP).

Finally, taking the limit when $t\to\infty$ in Eq. (11), the asymptotic temperature takes the form of,

$$T_\infty=\lim_{t\to\infty}T_s(t)=\frac{\mu}{\kappa}\,. \tag{13}$$

It should be pointed out that T_∞ is related to the mass flux of moisture through the Eqs. (9) and (11) given,

$$J=\frac{k}{\Delta r_s\lambda}\left(\delta+Nu\,(T_{amb}-T_\infty)\right)\,, \tag{14}$$

where the Nusselt number

$$Nu=\frac{h\Delta r_s}{k}=\frac{\kappa {\Delta r_s}^2}{\alpha} \tag{15}$$

was used. Note that if $J = 0$, and no other heat sources are present (metabolic heat, blood heat transport, etc.), after thermal equilibrium has been reached, $T_\infty = T_s = T_{int} = T_{amb}$. Therefore, δ must be equal to 0.
If κ and T_∞ could be derived from the thermography image, it would be possible to obtain a spatial distribution (a "map") of J, adapted to the local heat transfer condition. In that case, it would be convenient to write, in terms of the image pixel coordinates i and j,

$$J(i,j) = \frac{k}{\Delta r_s \lambda}\left(\delta + \frac{{\Delta r_s}^2}{\alpha}\kappa(i,j)\left(T_{amb} - T_\infty(i,j)\right)\right), \tag{16}$$

where $T_\infty(i,j)$ is an appropriately selected asymptotic thermal image. This procedure also requires the determination of a "map" of $\kappa(i,j)$, otherwise, a fix value should be obtained from fitting the thermal data, as was described previously using Eq. (11). The "map" of $\kappa(i,j)$ could be derived by averaging several measures of the expression,

$$\kappa(i,j) = -\frac{1}{(t-t_i)} ln\left(\frac{T_s(t)(i,j) - T_\infty(i,j)}{T_i(i,j) - T_\infty(i,j)}\right), \tag{17}$$

at different times during exponential decay or recovery, where $T_i(i,j)$ is a suitable initial thermal image, and $T_s(t)(i,j)$ is a thermal image at time t. Thermal properties (such as thermal conductivity, diffusivity, etc.) of biological tissues samples and for some mammalian species can be found in.[43–46] However, to our knowledge, there are no published data related to the thermophysical properties of the hamster cheek pouch. Poppendiek *et al.*[47] have suggested that tissues may be considered more accurately for thermal analysis as being composed of water, protein and fat. Based on these references and under this assumption, Table 1 shows the values of the assumed parameters used in the hamster cheek pouch model. Others thermophysical parameters shown in Table 1 were taken from[43–47] or determined experimentally, such as the temperature difference δ (measured).

Parameters	Value	Unit
Thermal diffusivity, α	1.3×10^{-7}	$m^2 s^{-1}$
Thermal conductivity, k	0.5	W $m°K^{-1}$
Density $\times$ specific heat, $k/\alpha = \rho C_p$	3.84×10^6	$m^{-2}s^{-2}$
Heat of evaporation, λ_W	2.26×10^6	J Kg^{-1}
Heat of sorption, λ_s	2.28×10^6	J Kg^{-1}
Thickness of the cheek pouch, Δr_s	0.001	m
Temperature difference, δ	2	°C

Table 1: Parameters values used in the hamster cheek pouch model based on published data.[43–47]

4. RESULTS AND DISCUSSION

In Section 4.1 we will describe the tissue thermal responses and determine each characteristic time constant, τ, for the non-irradiated groups (normal, precancerous tissue and tumor). We will then compare these results against the irradiated animals to find out if irradiation could be able to modify these values (Section 4.1.1). According to the case, a statistical analysis will be performed. A paired t-test analysis, will be applied to datasets obtained before and after the provocation test in the same trials, and the unpaired t-test analysis will be used in case of comparison of two different groups. For multiple comparisons, one-way analysis of variance (ANOVA) followed by Tukey's *post-hoc* test will be used. All statistical tests were considered statistically significant if P was less than or equal to 0.05. Using the MATLAB® statistics function "multcompare", a multiple pairwise comparison of the group mean values was made in each phase.
In Section 4.2 a preliminary study of the use of the mass flux moisture maps, J, in precancerous tissue and tumors will be discussed.

4.1 Tissue thermal response and its characteristic time constant τ

The thermal responses of the studied tissues will be presented using the absolute temperature values or with a dimensionless temperature, T^*, given by

$$T^* = 1 - \frac{T - T_i}{T_\infty - T_i}\,, \tag{18}$$

where T_i and T_∞ are the initial and final (asymptotic) temperature, respectively, in each phase of the experiment. It should be pointed out that the $T^*(t)$ curve behaves as $T(t)$. In Figure 4, the dimensionless thermal responses for normal tissue and tumor are shown, together with a "representative" synthetic curve. It was constructed based on Equation (11) using a characteristic time constant obtained averaging the τ values of each group and phase. A simple inspection of the plots reveals a different behavior between normal and tumor temperature curves in the PT region and, consequently, in the RP.

Figure 4 shows that 100% of the normal (non-cancerized) hamster cheek pouches ($n = 12$) exhibit identical thermal behavior named as, "normal thermal response". In the case of tumors, 100% of the curves ($n = 10$) exhibit a "tumor thermal response".

When the hamster cheek pouch is everted out of the mouth (TEP), both tumor and normal tissue temperature decay exponentially with time since they have an initial temperature higher than the ambient. It should be pointed out that in our experiment we observed that both tissues had a final temperature (in TEP) which is lower than the ambient temperature. The former case could be explained by superficial water evaporation. If no cooling process is present in the tissue, ambient temperature would be the minimum possible achievable value.

Meanwhile, during the PT, the temperature in normal tissue increases exponentially with time but tumor temperature decreases rapidly and significantly. Particularly, for normal tissue (Figure 4.a) this local warming response is due to the application of the air current at ambient temperature (26 ± 2 °C). The PT forces the normal tissue to attain thermal equilibrium with the ambient temperature. In the case of the tumor (Figure 4.b), on the other hand, the PT abruptly decreases its temperature due to evaporative cooling. It is well known that tumor vessels are characteristically dilated, saccular and tortuous and exhibit large interendothelial cell junctions, increased numbers of fenestrations, and lack of normal basement membrane.[48] The permeable and fragile tumor vessels cause hemorrhages and edema,[49] enhancing the evaporative cooling effect in tumor than in normal tissue.

Finally, after the PT, both tissues have no external stimuli and start a recovery process to their natural equilibrium. These processes are exponentially increasing and decreasing for tumor and normal tissue, respectively. The asymptotic temperature does not necessarily have to be equal to ambient temperature, but will depend on external and internal factors.[4]

In the case of the precancerous tissue, the thermal response varied between the cancerization protocols 1 and 2. In Protocol 1, 100% of the animals ($n = 5$) showed a "normal thermal response". Instead, in Protocol 2, in some cases, two thermal responses were found in the same pouch, depending on the ROI analyzed: 37.5% of the animals (3/8) showed "tumor thermal response" only and 62.5% of the animals (5/8) showed "tumor thermal response" and at least one "no thermal response", which corresponds to a curve that does not have an exponential behavior (both in PT and RP) and is insensitive to the thermal stimulus. No "normal response" was found in animals cancerized with Protocol 2. Note that Protocol 2 had twice the total amount of DMBA administrated in Protocol 1 (Figure 1). Histological and tumor development studies showed that Protocol 1 induces premalignant lesions and developed tumors in more than 90 % of the animals at 8 months follow-up. Instead, Protocol 2 induces a more aggressive precancerous tissue in terms of tumor development, i.e., 90 % of the animals with tumors at one month follow-up, and a more hypersensitive precancerous tissue than Protocol 1.[22,36]

As it was previously described, the temperature varied exponentially with time, thus, the characteristic time constant (τ) was determined. Table 2 shows the mean τ values in TEP and RP for each group of animals (See Figure 1). No characteristic time constant value was reported in PT since data points were spread out over this phase, showing a high standard deviation.

At the initial TEP, both normal tissue and tumor groups respond with equal characteristic time constant τ of 70 ± 21 and 79 ± 31 seconds*, respectively, showing no significant difference in the decay time constant. As it

*Values are expressed as mean ± standard deviation.

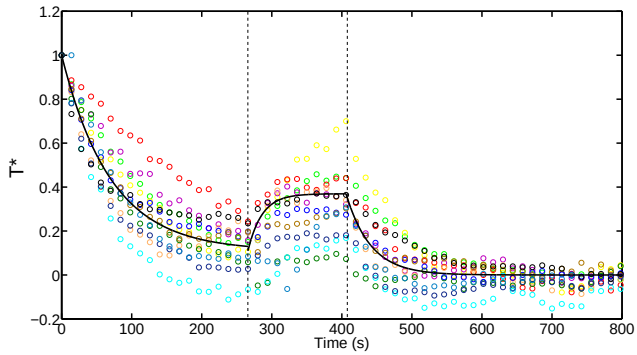

(a) Non-irradiated normal hamster cheek pouches (n=12): "Normal thermal response".

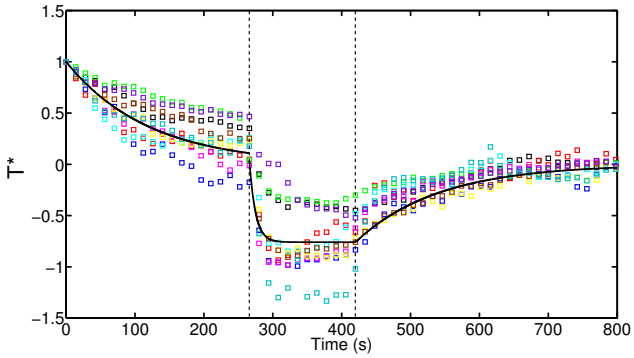

(b) Non-irradiated tumors ($n = 10$): "tumor thermal response".

Figure 4: Dimensionless experimental thermal responses as a function of time together with a "representative" synthetic curve (solid line). Vertical dashed lines separate the transient equilibrium phase (TEP), Provocation Test and Recovery Phase (RP).

was explained before, in TEP, both tumor and normal tissue are loosing their initial moisture condition, due to being inside the mouth. In the case of the RP, the rate at which the tissue recovers its temperature may or may not be equal to that found in the TEP. In RP, after drying the initial moisture condition in PT, we could be observing the internal and external factors that condition their response.

The rate at which the tissue recovers its temperature in RP may or may not be equal to that found in the TEP. In particular, in the case of the normal tissue, the decay time constant in the RP is half its value in the TEP (70 ± 21 *vs.* 35 ± 15 seconds, respectively). Note that the lower the decay time constant, the faster the heat loss in the tissue. Future studies will be performed to find out which internal factors would be involved in this thermal behavior. In the case of tumors, the recovery time constant in RP is equal to the decay time constant in TEP (79 ± 31 and 71 ± 12 seconds, in TEP and RP, respectively). In this case τ values for TEP and RP can not be compared because they reflect different thermal behaviors: In TEP the tumor is getting colder whereas in RP the tumor is getting hotter.

In the case of the precancerous tissue (Protocol 1), the τ values in TEP and RP are not significantly different to the normal tissue values (See Table 2). We previously showed that precancerous tissue from protocol 1 exhibited a normal tissue thermal response. As to Protocol 2, the time constant in TEP was 69 ± 41 seconds, similar to normal and precancerous tissue (Protocol 1) values. Unfortunately, we were not able to determine the τ value for RP for Protcocol 2 since no exponential curve fitted the data.

Tissue	Cancerization	Treatment	Mean ± SD	
			TEP	RP
Normal	Non-cancerized	Non-irradiated ($n = 12$)	70 ± 21	35 ± 15
		BNCT ($n = 6$)	55 ± 25	84 ± 19
Precancerous	Protocol 1	Non-irradiated ($n = 5$)	66 ± 28	42 ± 12
	Protocol 2	Non-irradiated ($n = 8$)	69 ± 41	Does not fit
		BO ($n = 6$)	79 ± 27	71 ± 11
		BNCT ($n = 5$)	145 ± 45	198 ± 68
Tumor	Protocol 2	Non-irradiated ($n = 10$)	79 ± 31	71 ± 12
		BO ($n = 4$)	75 ± 12	115 ± 48
		BNCT ($n = 5$)	140 ± 53	137 ± 43

Table 2: Mean τ values in the transient equilibrium phase (TEP) and recovery phase (RP) for each group of animals and treatments (See Figure 1). Values are expressed as mean ± standard deviation. Units are in seconds.

4.1.1 Multiple comparisons of the characteristic time constant between non-irradiated and irradiated groups

In this section, we will calculate the characteristic time constant for the irradiated groups and then compare these values with the characteristic time constants of the non-irradiated groups (See Figure 1). In particular, we will analyze if the τ value changes when the tissue is irradiated with BNCT or BO. As it was explained above, the BO group was performed to study BNCT background dose, i.e. without the boron dose component.
Table 2 and Figure 5 show τ values in TEP and RP for normal tissue (a) and tumor (b), BNCT treated or non-treated. For normal tissues during TEP, there is no significant difference in τ value between treated with BNCT or not treated (55 ± 25 *vs.* 70 ± 21 seconds, respectively). In RP, τ increases significantly its value (inversely to non-irradiated normal tissue, explained in Section 4.1. Although no macroscopically radiation adverse effects were seen in irradiated normal tissue, τ value increased in RP *vs.* τ value in RP for non irradiated normal tissue. This difference in tau values could be explained by a reduction in blood flow due to irradiation as it was previously reported in.[50]
Figure 6 shows a multicomparison study between tumors that were no irradiated, or treated with BNCT and Beam Only (BO). In TEP, the BNCT group has a mean τ value significantly different (p-value of 0.0270) from BO and non-irradiated groups (Figure 6.a). In the RP (Figure 6.b), only the mean τ value of the BNCT treated tumors and the non-irradiated tumors are significantly different (p-value of 0.0121) (BNCT and BO intervals overlap). In both TEP and RP, BNCT treated tumors exhibited the highest τ value. Irwin et al. mentioned that the blood supply to the region is reduced following human oral carcinoma irradiation.[16] This could explained the increased τ value found in the irradiated tumors, leading to slower changes in temperature. It is noteworthy that, the BNCT treated tumor group had an overall response significantly higher than the BO treated tumor group (93 % and 38 %, respectively).[36]

In the case of the irradiated versus non-irradiated precancerous tissue, we will only describe the results of Protocol 2 because Protocol 1 was not irradiated in this work. In TEP, non-irradiated and BO groups exhibited similar τ values and they were lower than the τ value of the BNCT group (69 ± 41 and 79 ± 27 versus 145 ± 45, respectively). In RP, the τ value for BNCT treated precancerous tissue was higher than the τ value for the BO group (Table 2). Macroscopic follow up of the animals showed no radiotoxicity in the BO group whereas, for the BNCT group, the animals exhibited ulcers (discontinuity or break in mucosa of oral cavity[51]) and sometimes necrosis.[36] This radiotoxic lesions could be contributing to a slower temperature recovery, that is a higher τ value.

Figure 7 shows an example of mucositis in the hamster cheek pouch, in which ulcers and necrosis coexist in the same pouch. Using the infrared images (Figure 7.b) it was possible to determine the isotherm curves in

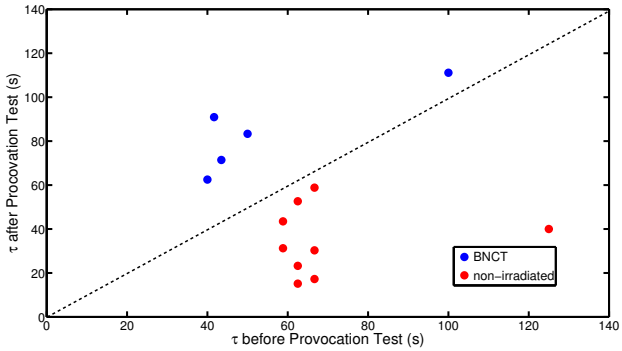

Figure 5: Characteristic time constant (τ) in the Transient Equilibrium Phase (TEP) and the Recovery Phase (RP), in BNCT treated and non-treated normal hamster cheek pouches. Points on the straight line $x = y$ have a τ value in TEP equal to that in RP.

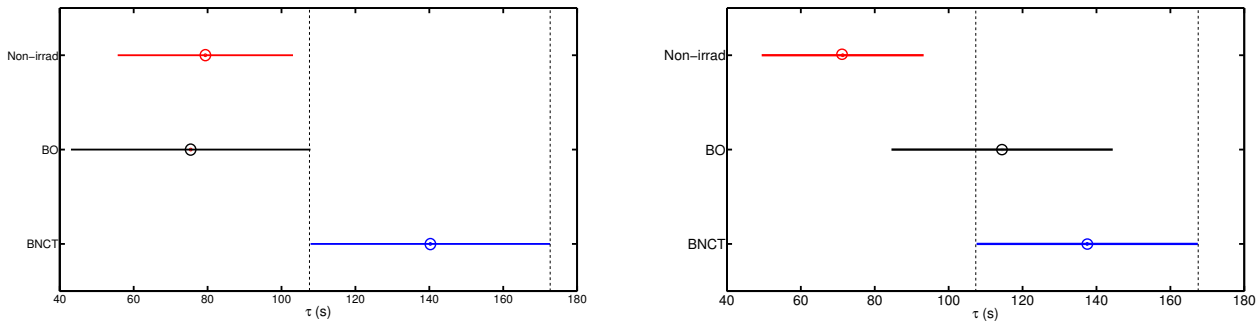

(a) Characteristic time constant in TEP.

(b) Characteristic time constant in RP.

Figure 6: Multiple comparison study between tumors that were no irradiated (Non-irrad), or treated with BNCT and Beam Only (BO).

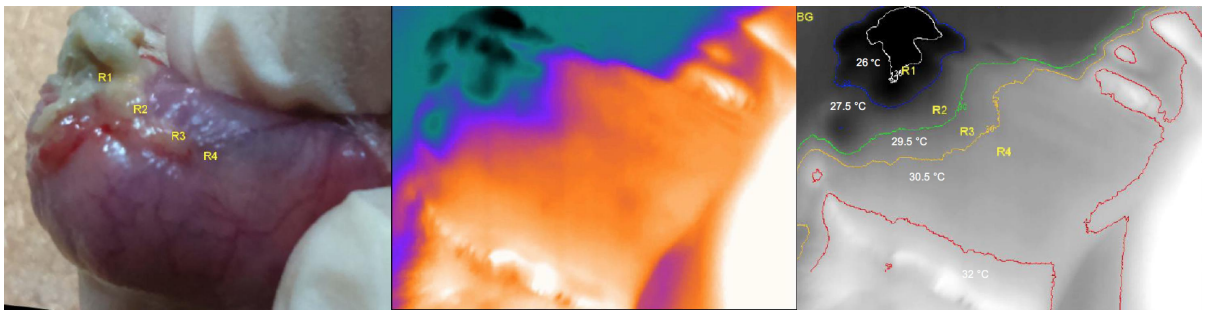

(a) Visible image.

(b) Infrared image.

(c) Isotherms.

Figure 7: BNCT treated hamster cheek pouch exhibiting severe mucositis in precancerous tissue.

a BNCT treated pouch, with different temperature regions (Figure 7.c). In particular, four regions of interest are shown in Figure 7.c (marked as R1, R2, R3, and R4) and their temperature curves in function of time were plotted (Figure 8). These temperatures decrease as the ROI approaches the main lesions of the tissue. We observed that R1, a region with necrosis surrounded by ulcers, had the greatest temperature variation during the PT. The final asymptotic temperature is significantly lower than the final asymptotic temperature for R4 (a

region with no ulcers nor necrosis). As can be seen in Figure 8 the temperature in the region with uclers and necrosis tends to the room temperature (showed in green).

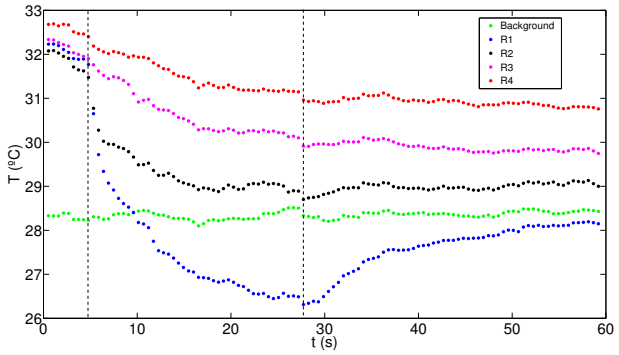

Figure 8: Temperature as a function of time during the provocation test and recovery phase in each region: R1, R2, R3, and R4 (See Figure 7.a).

4.2 Mass flux moisture maps J to explore radiotoxicity in precancerous tissue: preliminary study

The mass flux of moisture J [kg m^{-2} s^{-1}], derived in Eq. (14), was used to explore the radiotoxicity in the precancerous tissue. Figure 9 shows a "map" of J calculated according to Eq. (16) for (a) A non irradiated pouch, with no mucositis, (b) a cancerized pouch treated with BO, exhibiting mild mucositis (small ulcers) and (c) a cancerized pouch treated with BNCT exhibiting severe mucositis (ulcers and necrosis). In the first line, each visible image is presented. Second, third and forth photograph lines correspond to TEP, PT and RP images, respectively for each case (a,b and c).The J maps were calculated at the end of each phase. It should be pointed out that the map can only be read in the tissue region, while the values found in the background are not realistic (because the parameters involved in the calculation were not defined there). The spatial distribution of the moisture flux in both TEP and RP is given by the geometry of the pouch.
the animal's breathing.
In the non-irradiated precancerous tissue with no mucositis (a), when the airflow is applied, the mass moisture transfer increases in the whole pouch and up to a factor of 2 in the tumor ($J > 0.4$ g m^{-2} s^{-1}). Since the animal was not exposed to radiation, the J distribution in the tissue, during the PT, is quite homogenous ($J \sim 0.3$ g m^{-2} s^{-1}), except in the tumor. Both observations are probably due to the higher water evaporation described in section 4.1 in tumor vs normal tissue. A second "hot" spot can be detected in the image, that might be related to the animal's breathing.
As to figures (b) and (c), the J value differences are enhanced by the provocation test as in figure (a). We observed that not only tumors but also tissue injuries such as inflammation, ulcers and necrosis can be detected in the J map. The highest values of J occur in those regions of the pouch bearing ulcers and necrosis. As to tumors we observed, as in (a), that the mass moisture transfer increases by a factor of 2 (or higher) than the tissue injuries factor.

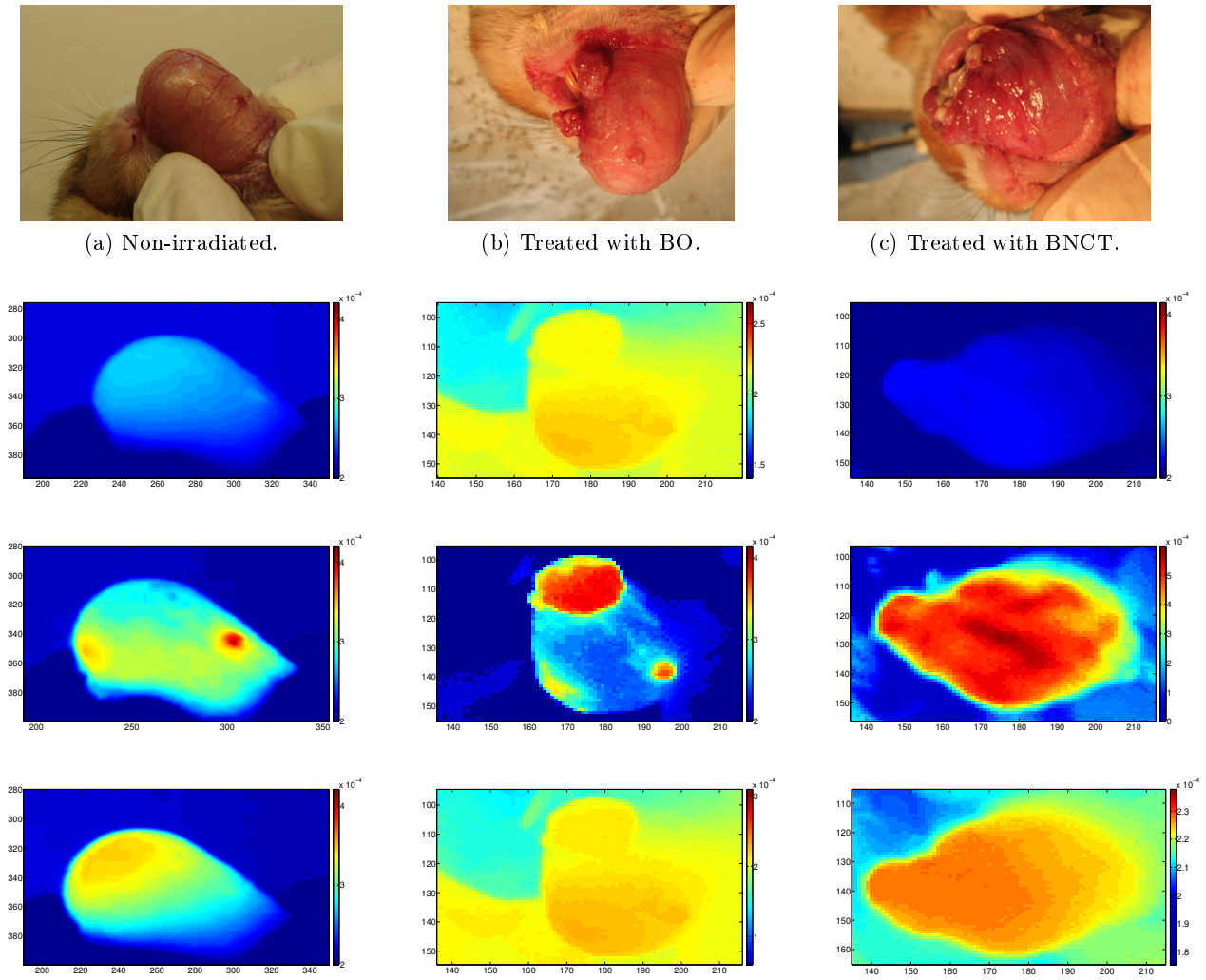

(a) Non-irradiated. (b) Treated with BO. (c) Treated with BNCT.

Figure 9: Hamster cheek pouch cancerized with Protocol 1 (a) and 2 (b and c) exhibiting in precancerous tissue: (a) No mucositis, (b) Mild mucositis: with small ulcers and (c) Severe mucositis: ulcers and necrosis. Mass flux of moisture maps (kg m^{-2} s^{-1}), were calculated at the end of the Transient Equilibrium Phase (second line), Provocation Test (third line), and Recovery Phase (forth line) are shown.

ulcers and necrosis). As to tumors, we observed the greatest surface moisture loose, reaching differences by a factor of 2 or higher.

5. CONCLUSIONS

In this work, we have studied 61 hamsters with Dynamic Infrared Imaging (DIRI). We analyzed the thermal responses (temperature vs time) of normal, precancerous tissue and tumor, without irradiation or with Beam only (BO) and BNCT treatments, in different experimental phases: Transient Equilibrium Phase (TEP), Provocation Test (PT) and Recovery Phase (RP). We used a mathematical model that contemplates the loss of heat by diffusion and convection and evaporative cooling that allowed us to obtain a specific parameter that characterized the exponentially decaying or recovering thermal responses: τ, the characteristic time constant. To our knowledge, the characteristic time constant of thermal responses in biological tissues had never been reported. Using this model we proposed a simple mathematical procedure that allowed us to explore the mass flux of moisture, J, as

a degree of evaporation occurring on the tissue surface.

As to the thermal responses, we were able to characterized "normal thermal responses" for normal tissue and "tumor thermal responses" for tumor. The fact that: a) a less aggressive precancerous tissue (Protocol 1) showed a "normal thermal response" with τ values similar to a normal tissue, and b) that a more aggressive precancerous tissue (Protocol 2) had no "normal thermal responses". Although more complementary studies are needed, we could propose DIRI as a predictive tool for the evaluation of the aggressiveness of precancerous tissue, in terms of tumor development.

When analyzing τ values for tumor irradiated with BNCT and BO, BNCT was able to increase the τ value in both TEP and RP. Whereas, BO group, had only increase τ value in RP. When we analyzed tumor response in each group, we reported that the BO group had a significantly lower tumor response than the BNCT treated tumors.[36] These results could be hypothesizing that τ value could be a possible predictor of tumor response. Future studies, in which tumor macroscopic follow up with DIRI would help to reinforce this idea. Other studies on tumors[5] showed that thermographic imaging was able to monitor the presence and progression of xenograft tumors and proposed this technique to assess their response to anticancer therapies.

In previous studies (for example[17]), infrared thermography was used to evaluate inflammation of the oral tissue. Our aim was to study mucositis and calculate two parameters that could also be helpful to describe mucositis in oral mucosa. For that aim, we studied mucositis in the hamster cheek pouch, which is a widely accepted model of oral mucositis.[26] In this work we added a stimulus (an air stream at ambient temperature) applied directly to the region of interest, to enhance the temperature responses of the tissues. We observed how τ values in TEP and RP were higher in precancerous tissue treated with BNCT, exhibiting ulcers and necrosis. As to the mass flux moisture maps, they showed how evaporative cooling is significantly increased in tumors and radiotoxic lesions in the PT. It should be noticed that this effect can be increased or decreased by the relative humidity in the ambient, since the evaporative heat loss depends on the concentration of steam between the tissue surface and the ambient. A relative humidity of 100 % would completely suppress evaporative cooling from the tissue. This first approximation of the mass flux moisture maps provides new insights to the evaporative cooling in the biological model. Future investigations should include relative humidity ambient corrections in our calculations.

While much work remains to be done, it is clear that DIRI is a very useful tool that provides non-invasively additional and complementary information on the normal and abnormal status of the tissues and their response to BNCT treatment. The fact that thermal imaging could be able to monitor tumor development and malignancy of the surrounding precancerous tissue would be an advantage in assessing their response to cancer therapies.

ACKNOWLEDGMENTS

This work was partially supported by CONICET. The authors thank the oral exposition and acknowledge the valuable contribution by Andrés E. Rozlosnik to this work.

REFERENCES

[1] Di Carlo, A., "Thermography and the possibilities for its applications in clinical and experimental dermatology," *Clinics in Dermatology* **13**, 329–336 (1995).

[2] Santa Cruz, G. A., González, S. J., Bertotti, J., and Marín, J., "First application of dynamic infrared imaging in boron neutron capture therapy for cutaneous malignant melanoma," *Med. Phys.* **36**, 4519–4529 (2009).

[3] Santa Cruz, G. A., González, S. J., Dagrosa, A., Schwint, A. E., Carpano, M., Trivillin, V. A., Boggio, E. F., Bertotti, J., Marín, J., Monti Hughes, A., Molinari, A. J., and Albero, M., "Dynamic infrared imaging for biological and medical applications in boron neutron capture therapy," in [*Thermosense: Thermal Infrared Appl. XXXIII*], Safai, M. and Brown, J. R., eds., **8013**, 7–25, SPIE, Orlando, Florida, USA (2011).

[4] Biagioni, P. A., Longmore, R. B., McGimpsey, J. G., and Lamey, P. J., "Infrared thermography. its role in dental research with particular reference to craniomandibular disorders," *Dentomaxillofac. Radiol.* **25(3)**, 119–124 (1996).

[5] Song, C., Appleyard, V., Murray, K., Frank, T., Sibbett, W., Cuschieri, A., and Thompson, A., "Thermographic assessment of tumor growth in mouse xenografts," *Int J Cancer* **121(5)**, 1055–1058 (2007).

[6] Chojnowski, M., "Infrared thermal imaging in connective tissue diseases.," *Reumatologia* **55(1)**, 38–43 (2017).

[7] Trivillin, V. A., Heber, E. M., Nigg, D. W., Itoiz, M. E., Calzetta, O., Blaumann, H., Longhino, J., and Schwint, A. E., "Therapeutic success of boron neutron capture therapy (BNCT) mediated by a chemically non-selective boron agent in an experimental model of oral cancer: a new paradigm in BNCT radiobiology," *Radiat Res* **166**, 387–396 (2006).

[8] Kellogg, D. L., "In vivo mechanisms of cutaneous vasodilation and vasoconstriction in humans during thermoregulatory challenges," *J. Appl. Physiol.* **100(5)**, 1709–1718 (2006).

[9] Arora, N., Martins, D., Ruggerio, D., Tousimis, E., Swistel, A. J., Osborne, M. P., and Simmons, R. M., "Effectiveness of a noninvasive digital infrared thermal imaging system in the detection of breast cancer," *The American Journal of Surgery* **196**, 523–526 (2008).

[10] Hildebrandt, C., Raschner, C., and Ammer, K., "An overview of recent application of medical infrared thermography in sports medicine in austria," *Sensors* **10**, 4700–4715 (2010).

[11] Çetingül, M. P. and Herman, C., "Quantification of the thermal signature of a melanoma lesion," *Clinics in Dermatology* **13**, 329–336 (2011).

[12] Bhavani Bharathi, G., Francis, S. V., Sandeep, M. S. D., and Jaipurka, D., "Feature analysis for abnormality detection in breast thermogram sequences subject to cold stress," in [*Proceedings of The National Conference on Man Machine Interaction 2014*], Loew, M. H., ed., *NCMMI 2014*, 15–21 (2014).

[13] Ferlay, J., Soerjomataram, I., Ervik, M., Dikshit, R., Eser, S., Mathers, C., Rebelo, M., Parkin, D. M., Forman, D., and Bray, F., "Globocan 2012 v1.0, cancer incidence and mortality worldwide: Iarc cancerbase no. 11 [internet].," *Lyon, France: International Agency for Research on Cancer* (2013).

[14] Machiels, J. P., Lambrecht, M., Hanin, F. X., Duprez, T., Gregoire, V., Schmitz, S., and Hamoir, M., "Advances in the management of squamous cell carcinoma of the head and neck," *F1000Prime Rep* **6**, 44 (2014).

[15] Kato, I., Ono, K., Sakurai, Y., and Yura, Y., "Effectiveness of bnct for recurrent head and neck malignancies," *Applied Radiation and Isotopes* **61(5)**, 1069–73 (2004).

[16] Irwin, J. W., Xavara, B. S., Bartley, H., and Raze, J. A., "Intraoral thermography," *Oral Surg.* **32(5)**, 724–730 (1971).

[17] White, B. A., Lockhart, P. B., Connolly, S. F., and Sonis, S. T., "The use of infrared thermography in the evaluation of oral lesions," *Clinical Techniques* **113**, 783–786 (1986).

[18] Kreimann, E., Itoiz, M. E., Dagrosa, A., Garavaglia, R., Farías, S., Batistoni, D., and Schwint, A. E., "The hamster cheek pouch model of oral cancer for boron neutron capture therapy studies: selective delivery of boron by boronophenylalanine," *Cancer Res* **61**, 8775–8781 (2001).

[19] Kreimann, E. L., Itoiz, M. E., Longhino, J., Blaumann, H., Calzetta, O., and Schwint, A. E., "Boron neutron capture therapy for the treatment of oral cancer in the hamster cheek pouch model," *Cancer Res* **61**, 8638–8642 (2001).

[20] Monti Hughes, A., Aromando, R. F., Pérez, M. A., Schwint, A. E., and Itoiz, M. E., "The hamster cheek pouch model for field cancerization studies," *Periodontol 2000* **67**, 292–311 (2015).

[21] Vairaktaris, E., Spyridonidou, S., Papakosta, V., Vylliotis, A., Lazaris, A., Perrea, D., Yapijakis, C., and Patsouris, E., "The hamster model of sequential oral oncogenesis. review," *Oral Oncol* **44**, 315–324 (2008).

[22] Heber, E. M., Monti Hughes, A., Pozzi, E. C., Itoiz, M. E., Aromando, R. F., Molinari, A. J., Garabalino, M. A., Nigg, D. W., Trivillin, V. A., and Schwint, A. E., "Development of a model of tissue with potentially malignant disorders (pmd) in the hamster cheek pouch to explore the long-term potential therapeutic and/or toxic effects of different therapeutic modalities," *Arch Oral Biol* **55**, 46–51 (2010).

[23] Simple, M., Suresh, A., Das, D., and Kuriakose, M., "Cancer stem cells and field cancerization of oral squamous cell carcinoma," *Oral Oncology* **51(7)**, 643–651 (2015).

[24] Monti Hughes, A., Pozzi, E. C., Thorp, S., Garabalino, M. A., Farías, R. O., González, S. J., Heber, E. M., Itoiz, M. E., Aromando, R. F., Molinari, A. J., Miller, M., Nigg, D. W., Curotto, P., Trivillin, V. A., and Schwint, A. E., "Boron neutron capture therapy for oral precancer: proof of principle in an experimental animal model," *Oral Dis* **52**, 789–795 (2013).

[25] Jaiswal, G., Jaiswal, S., Kumar, R., and Sharma, A., "Field cancerization: concept and clinical implications in head and neck squamous cell carcinoma," *J Exp Ther Oncol* **10**, 209–214 (2013).

[26] Bowen, J. M., Gibson, R. J., and Keefe, D. M. K., "Animal models of mucositis: implications for therapy," *J Support Oncol* **9**, 161–168 (2011).

[27] Jensen, S. B. and Peterson, D. E., "Oral mucosal injury caused by cancer therapies: current management and new frontiers in research," *J Oral Pathol Med* **43(2)**, 81–90 (2014).

[28] Kankaanranta, L., Seppala, T., Koivunoro, H., Saarilahti, K., Atula, T., Collan, J., Salli, E., Kortesniemi, M., Uusi-Simola, J., Valimaki, P., Makitie, A., Seppanen, M., Minn, H., Revitzer, H., Kouri, M., Kotiluoto, P., Seren, T., Auterinen, I., Savolainen, S., and Joensuu, H., "Boron neutron capture therapy in the treatment of locally recurred head-and-neck cancer: final analysis of a phase i/ii trial," *Int J Radiat Oncol Biol Phys* **82(1)**, e67–75 (2012).

[29] Wang, L. W., Chen, Y. W., Ho, C. Y., Liu, Y. W. H., Chou, F. I., Liu, Y. H., Liu, H. M., Peir, J. J., Jiang, S. H., Chang, C. W., Liu, C. S., Wang, S. J., Chu, P. Y., and Yen, S. H., "Fractionated BNCT for locally recurrent head and neck cancer: Experience from a phase i/ii clinical trial at tsing hua open-pool reactor," *Appl Radiat Isot* **88**, 23–27 (2014).

[30] Koohi-Hosseinabadi, O., Andisheh-Tadbir, A., Bahadori, P., Sepehrimanesh, M., Mardani, M., and Tanideh, N., "Comparison of the therapeutic effects of the dietary and topical forms of zizyphus jujuba extract on oral mucositis induced by 5-fluorouracil: A golden hamster model," *J Clin Exp Dent* **7(2)**, e304–309 (2015).

[31] Perez, M. A., Raimondi, A. R., and Itoiz, M. E., "An experimental model to demonstrate the carcinogenic action of oral chronic traumatic ulcer," *J Oral Pathol Med* **34**, 17–22 (2005).

[32] Lalla, R. V., "Alleviating mucositis: are we on track for a novel therapeutic," *Expert Review of Gastroenterology & Hepatology* **9**, 127–128 (2015).

[33] Hughes, A. M., Heber, E. M., Pozzi, E., Nigg, D. W., Calzetta, O., Blaumann, H., Longhino, J., Nievas, S. I., Aromando, R. F., Itoiz, M. E., Trivillin, V. A., and Schwint, A. E., "Boron neutron capture therapy (BNCT) inhibits tumor development from precancerous tissue: an experimental study that supports a potential new application of BNCT," *Appl Radiat Isot* **67(7-8 Suppl)**, S313–317 (2009).

[34] Heber, E. M., Hawthorne, M. F., Kueffer, P. J., Garabalino, M. A., Thorp, S. I., Pozzi, E. C., Monti Hughes, A., Maitz, C. A., Jalisatgi, S. S., Nigg, D. W., Curotto, P., Trivillin, V. A., and Schwint, A. E., "Therapeutic efficacy of boron neutron capture therapy mediated by boron-rich liposomes for oral cancer in the hamster cheek pouch model," *Proc Natl Acad Sci U S A* **111**, 16077–16081 (2014).

[35] Molinari, A. J., Pozzi, E. C. C., Monti Hughes, A., Heber, E. M., Garabalino, M. A., Thorp, S. I., Miller, M., Itoiz, M. E., Aromando, R. F., Nigg, D. W., Quintana, J., Santa Cruz, G., Trivillin, V., and Schwint, A., "Sequential boron neutron capture therapy (BNCT): A novel approach to BNCT for the treatment of oral cancer in the hamster cheek pouch model," *Radiation Research* **175(4)**, 463–472 (2011).

[36] Monti Hughes, A., Longhino, J., Boggio, E., Medina, V. A., Lamas, D. M., Garabalino, M., Heber, E., Pozzi, E., Itoiz, M., Aromando, R., Nigg, D., Trivillin, V., and Schwint, A., "2016 translational BNCT studies in the hamster cheek pouch model of oral cancer at the new configuration of the ra-6 nuclear reactor," *ICNCT 17* (2016).

[37] Teketee, J., "Spectral emissivity of skin and pericardium," *Phys. Med. Biol.* **18**, 686–694 (1973).

[38] Togawa, T., "Non-contact skin emissivity: measurement from reflectance using step change in ambient radiation temperature," *Clin. Phys. Physiol. Meas.* **10(1)**, 39–48 (1989).

[39] Baini, R. and Langrish, T. A. G., "Choosing an appropriate drying model for intermittent and continuous drying of bananas," *Journal of Food Engineering* **79**, 330–343 (2007).

[40] Tolaba, M. P., Aguerre, R. J., and Suárez, C., "Modeling cereal grain drying with variable diffusivity," *Cereal Chem* **74**, 842–845 (2007).

[41] Suárez, C. and Viollaz, P., "Shrinkage effect on drying behavior of potato slabs," *Journal of Food Engineering* **13**, 103–114 (1991).

[42] Wan, J. and Langrish, T. A. G., "A numerical simulation for solving the diffusion equations in the drying hardwood timber," *Drying Technology* **13(3)**, 330–343 (783–799).

[43] Holmes, K. and Chen, M. M., "Local thermal conductivity of para-7 fibrosarcoma in hamster," in [*Advances in Bioengineering, ASME*], 147–149 (1979).

[44] Valvano, J. W., Allen, J. T., and Bowman, H. F., "The simultaneous measurement of thermal conductivity, thermal diffusivity, and perfusion in small volumes of tissue," *J. Biomech. Eng.* **106(3)**, 192–197 (1884).

[45] Duck, F. A., [*Physical Properties of Tissue: A Comprehensive Reference Book*], Academic Press, London (1990).

[46] El-Brawany, J., Nassiri, D. K., Terhaar, G., Shaw, A., Rivens, I., and Lozhken, K., "Measurement of thermal and ultrasonic properties of some biological tissues," *Journal of Medical Engineering & Technology* **33(3)**, 249–256 (2009).

[47] Poppendiek, H. F., Randall, R., Breeden, J., Chambers, J. E., and Murphy, J. R., "Thermal conductivity measurements and predictions for biological fluids and tissues," *Cryobiology* **3**, 318–327 (1966).

[48] Molinari, A. J., Aromando, R. F., Itoiz, M. E., Garabalino, M. A., Hughes, A. M., Heber, E. M., OZZI, E. C. P., Nigg, D. W., and amd A. E. Schwint, V. A. T., "Blood vessel normalization in the hamster oral cancer model for experimental cancer therapy studies," *Anticancer Research* **32**, 2703–2709 (2012).

[49] Dejana, E. and Orsenig, F., "Endothelial adherens junctions at a glance," *Journal of Cell Science* **126**, 2545–2549 (2013).

[50] Roth, N. M., Sontag, M. R., and Kiani, M. F., "Early effects of ionizing radiation on the microvascular networks in normal tissue.," *Radiat Res.* **151(3)**, 270–7 (1999).

[51] Lee, D. Y., Kim, H.-B., Shim, I. K., Kanai, N., Okano, T., and Kwon, S. K., "Treatment of chemically induced oral ulcer using adipose-derived mesenchymal stem cell sheet," *J Oral Pathol Med* , in press (2016).